ITEMS FOR UNRUH DATA REPOSITORY

i) List of Data Repository Tables

Table DR-1: SHRIMP-RG U-Pb age data for detrital zircons from Mt. Diablo sample MD96-4.

Table DR-2: Fission track sample locality, counting, and age data from Mt. Diablo area.

Table DR-3: (U-Th)/He analytical data for individual apatite grains from samples from the Mt. Diablo area.

Table DR-4: Modeling of (U-Th)/He ages from the Mt. Diablo area.

ii) Figure Captions for Figures Included Within the Data Repository

Figure DR-1: Histograms of fission track lengths from ten additional samples. Data from seven of these samples, along with fission track dpar data included in Figure DR2, were used as inputs into fission track modeling programs. The modeled output histories from these samples are shown in Figure DR3.

Figure DR-2: Plots of the fission track dpar parameter for each track length measurement and each single-grain age determination for sixteen fission track samples. The dpar parameter (Donelick, 1993; Ketcham et al., 1999, 2000) correlates with the annealing kinetics of the apatite grains and is used as an input for fission track modeling shown in Figures 9 and DR3. For the modeling, the approach taken was to divide the data into three populations based on dpar, such that most of the data fell in the middle population and the other two populations were dominated by outliers. The low and high dpar

populations (shaded) were then discarded and only the central population was modeled, using its midpoint dpar value. Dpar data were not collected from Franciscan samples 95SF-004 and 95SF-005 because only 13 and 9 track lengths, respectively, were available for measurement in these samples (Figure 9). Sample 97SF-006, from the "Knoxville" unit of the Great Valley Group, exhibits a wide spread in dpar values and in addition its structural setting is poorly understood. For these reasons, these three samples were not modeled.

Figure DR-3: Fission track modeling plots for seven of the samples shown in Figure DR1. See Figure 11 for key.

Figure DR-4: Plots of degree of resetting of single-grain (U-Th)/He ages versus two proxies for the magnitude of alpha-decay-induced radiation damage in individual apatite grains. Degree of resetting is the same as in Figure 9B. In (A), X values are effective U (eU) for each grain; eU = U + 0.235*Th (concentrations in parts per million), as defined by Shuster et al., 2006. eU is an accurate proxy for the current mean rate of alpha decay per unit volume within each grain. In (B), X values are the product of eU and eTime. eTime is He start age minus 3.5 m.y., as in Figure 9B. These X values are therefore a tentitive proxy for the current mean density of radiation damage within each grain. Shuster et al. (2006) proposed that radiation damage causes retardation of He diffusion by "trapping" He within damaged zones. Such a model predicts a positive correlation (positive slope) in plots such as these, with more damaged grains yielded older ages. However, these plots show no apparently correlation. This indicates that the radiation

damage model does not explain the wide spread in single grain He ages observed at Mt Diablo. We therefore acribe the variable single-grain diffusion behavior observe in the Mt Diablo samples to some other unknown mechanism.

It should be noted that the model of Shuster et al. (2006) may require some minimum level of radiation damage before inducing detectable variations in single-grain ages. The levels of radiation damage in our samples are probably relatively low compared to examples cited by Shuster et al. (2006) and Green et al. (2006). Therefore, even though the radiation-damage model does not appear to explain our data, our data do not necessarily indicate that the radiation-damage model is incorrect.

It should also be noted that the magnitude of differences in single-grain diffusion parameters needed to explain our data (Figure 9C) are relatively small compared to the radiation-induced differences proposed by Shuster et al. (2006). They therefore probably represent some separate mechanism of unknown physical nature. Because the differences are small, they would be expected to cause variations in single-grain ages only under quite restricted time-temperature histories. Histories with late reheating to temperatures near the middle of the He partial retention zone (about 75°C), such as seen at Mt. Diablo, are most likely to cause detectable single-grain age variations.

Figure DR-5: We assume a kink-band-propagation style of folding (Suppe, 1983; Suppe and Medwedeff, 1990), and account for the effect of distributed simple shear in the fold limbs by using a graphical approach to transform pre-existing faults and bedding contacts

from the deformed to the undeformed state (DR-5a). Shearing of fold limbs during deformation is illustrated by comparing the geometry of the parallelogram defined by the A and B hinge lines in the deformed (DR-5a) and restored (DR-5b) states. We assume that shear during fold growth is accommodated by distributed reverse slip along planes parallel to dip of the fold limb; in general, these planes need not be parallel to bedding. In cross-section, the shear planes are lines of no finite extension. Intersections of bedding, faults and other features with these lines form a grid of points that is used graphically to map the deformed geometry (DR-5a) to the restored geometry (DR-5b). Although the distances between points along the lines are the same in both the deformed and restored states, the lengths and angular relationships of lines that connect these points between lines are different in the two states due to simple shear of the fold limb.

ADDITIONAL REFERENCES CITED ONLY IN DATA REPOSITORY ITEMS

Black, L.P, Kamo, S.L, Allen, C.M, Davis, D.W, Aleinikoff, J.N, Valley, J.W, Mundil, R., Campbell, I.H, Korsch, R.J, Williams, I.S, and Foudoulis, C., 2004, Improved 206Pb/ 238U microprobe geochronology by the monitoring of a trace-element-related matrix effect: SHRIMP, ID-TIMS, ELA-ICP-MS and oxygen isotope documentation for a series of zircon standards: Chemical Geology, v. 205, p. 115-140.

Dumitru, T.A., 1993, A new computer-automated microscope stage system for fission track analysis: Nuclear Tracks and Radiation Measurements, v. 21, p. 575-580.

Farley, K.A., Wolf, R.W., and Silver, L.T., 1996, The effects of long alpha-stopping distances on (U-Th)/He ages: Cosmochimica et Geochimica Acta, v. 60, p. 4223-4229.

Galbraith, R.F., 1981, On statistical models for fission track counts: Mathematical Geology, v. 13, p. 471-478.

Galbraith, R.F., and Laslett, G.M., 1993, Statistical models for mixed fission track ages: Nuclear Tracks and Radiation Measurements, v. 21, p. 459-470.

Green, P.F., 1981, A new look at statistics in fission-track dating: Nuclear Tracks and Radiation Measurements, v. 5, p. 77-86.

House, M.A., Farley, K.A., and Stockli, D., 2000, Helium chronometry of apatite and titanite using Nd-YAG laser heating: Earth and Planetary Science Letters, vol.183, pp.365-368.

Hurford, A.J., and Green, P.F., 1983, The zeta age calibration of fission-track dating: Chemical Geology, v. 41, p. 285-317.

Ireland, T.R., and Williams, I.S., 2003, Considerations in zircon geochronology by SIMS: Reviews in Mineralogy and Geochemistry, v. 53, p. 215-241.

Ketcham, R.A., Donelick, R.A., and Carlson, W.D., 1999, Variability of apatite fission-track annealing kinetics. 3. Extrapolation to geological time scales: American Mineralogist, v. 84, p. 1235-1255.

Laslett, G.M., Kendall, W.S., Gleadow, A.J.W., and Duddy, I.R., 1982, Bias in the measurement of fission track length distributions: Nuclear Tracks and Radiation Measurements, v. 6, p. 79-85.

Ludwig, K.R., 2001, Squid: Special Publication 2, Berkeley Geochronology Center, Berkeley, California.

Suppe, J., 1983, Geometry and kinematics of fault-bend folding: American Journal of Science, v. 283, p. 684-721.

Suppe, J., and Medwedeff, D.A., 1990, Geometry and kinematics of fault-propagation folding: Eclogae Geologicae Helvetiae, v. 83, p. 409-454.

Williams, I.S., 1997, U-Th-Pb geochronology by ion microprobe: Reviews in Economic Geology, v. 7, p. 1-35.

Table DR1. SHRIMP-RG U-Pb AGES OF DETRITAL ZIRCONS FROM MT. DIABLO SAMPLE MD96-4.

Zircon Grain Number	% com-mon 206Pb	ppm U	ppm Th	232Th /238U	207Pb corrected 206Pb /238U	1s err	207Pb corrected 206Pbr /238U Age	1s err	Uncor-rected 238U /206Pb	% err	Uncorrected 207Pb /206Pb	% err
7	0.73	215	61	0.29	.0167	####	**106.6**	**1.7**	59.52	1.6	.0539	4.9
10	0.65	282	115	0.42	.0168	####	**107.4**	**1.5**	59.14	1.4	.0533	4.6
24	0.61	271	139	0.53	.0170	####	**108.8**	**1.6**	58.40	1.4	.0530	4.6
22	0.24	141	77	0.56	.0225	####	**143.4**	**2.6**	44.36	1.8	.0508	5.8
4	0.47	240	112	0.48	.0238	####	**151.9**	**2.0**	41.74	1.3	.0529	4.2
1	0.05	167	74	0.46	.0249	####	**158.5**	**2.5**	40.16	1.6	.0496	5.1
29	-0.22	273	73	0.28	.0254	####	**161.7**	**2.0**	39.46	1.2	.0475	4.0
26	0.40	241	184	0.79	.0254	####	**161.8**	**2.1**	39.18	1.3	.0524	4.0
15	0.63	83	24	0.29	.0255	####	**162.4**	**3.8**	38.95	2.3	.0543	6.9
16	0.08	1012	1138	1.16	.0256	####	**162.9**	**1.0**	39.04	0.6	.0500	2.1
28	0.26	670	675	1.04	.0256	####	**163.2**	**1.2**	38.89	0.8	.0514	2.4
2	0.06	616	339	0.57	.0258	####	**164.2**	**1.3**	38.75	0.8	.0498	2.6
17	0.15	425	218	0.53	.0261	####	**165.9**	**1.6**	38.30	1.0	.0506	3.1
21	-0.22	686	755	1.14	.0262	####	**167.0**	**1.3**	38.18	0.8	.0476	2.5
25	0.16	986	1312	1.38	.0265	####	**168.5**	**1.1**	37.71	0.6	.0507	2.0
23	0.90	174	91	0.54	.0266	####	**169.3**	**2.7**	37.25	1.6	.0566	4.7
27	0.47	570	430	0.78	.0266	####	**169.4**	**1.4**	37.37	0.8	.0532	2.5
9	0.42	511	335	0.68	.0268	####	**170.6**	**1.5**	37.14	0.9	.0528	2.8
18	0.70	177	91	0.53	.0272	####	**172.7**	**2.5**	36.57	1.4	.0551	4.4
11	-0.01	703	443	0.65	.0275	####	**174.7**	**1.2**	36.41	0.7	.0495	2.2
14	0.16	649	425	0.68	.0275	####	**175.2**	**1.4**	36.25	0.8	.0508	2.5
3	0.25	226	106	0.49	.0277	####	**176.1**	**2.3**	36.02	1.3	.0516	4.1
20	0.32	215	99	0.47	.0277	####	**176.3**	**2.4**	35.95	1.3	.0522	4.2
12	0.29	234	116	0.51	.0286	####	**181.7**	**2.3**	34.87	1.3	.0520	4.0
6	-0.11	254	124	0.50	.0290	####	**184.1**	**2.2**	34.56	1.2	.0489	3.9
19	0.11	271	138	0.53	.0291	####	**185.1**	**2.2**	34.29	1.2	.0507	3.8
13	0.58	643	475	0.76	.0291	####	**185.2**	**1.4**	34.12	0.7	.0544	2.3
30	0.45	373	121	0.33	.0300	####	**190.8**	**1.9**	33.14	1.0	.0535	3.0
8	0.56	139	27	0.20	.0343	####	**217.2**	**3.3**	29.01	1.5	.0549	4.6
5	0.16	217	27	0.13	.0386	####	**244.3**	**2.8**	25.85	1.2	.0523	3.5

The following is a summary of key laboratory procedures. Zircons were separated using standard heavy liquid and magnetic methods (e.g., Dumitru, 2000). The final step of magnetic separation was completed using a Frantz Isodynamic separator with a current setting of 1.8 amps and a side slope of 5 degrees. Individual zircons grains were selected under the binocular microscope, embedded in epoxy, and ground and polished to a 1 micron finish to allow analysis of grain internal surfaces. Grain internal surfaces were imaged under cathodoluminescence (CL) and under reflected plane light.

Isotopic analyses were preformed in March 2006 on the SHRIMP-RG at the Stanford-USGS Microisotopic Analytical Center, using methods similar to Surpless et al. (2006). The spot size of the O2- primary beam was approximately 30-40 microns; each analysis consisted of four scans for each isotope mass. Concentrations were standardized against the CZ3 zircon standard (550 ppm U). Ages were standardized against the R33 zircon standard (419 Ma ID-TIMS age; Black et al., 2004). The operator analyzed 30 individual grains, using the images to attempt to sample the full range of zircon grain types present on the mount, rather than sampling at random. This strategy was selected because a key goal was to bracket the depositional age of the sample using the youngest zircons and because instrument time was limited. Data reduction followed the methods of Williams (1997) and Ireland and Williams (2003), using the Squid and Isoplot programs of Ludwig (2001, 2003).

After the age analyses were completed, the CL images and reflected light images were reexamined. This indicated that, for this sample, it was not possible to sort grains into different age populations based on the images alone.

TABLE DR2. FISSION TRACK SAMPLE LOCALITY, COUNTING, AND AGE DATA FROM MT. DIABLO AREA

Sample	Irradiation	Latitude	Longitude	No	Spontaneous		Induced		$P(\chi^2)$	Dosimeter		Age ± 1σ	
number	number	(North)	(West)	Xls	Rho-S	NS	Rho-I	NI	(%)	Rho-D	ND	(Ma)	
Great Valley Group Samples													
97SF-006	SU040-06	37° 54' 29"	121° 55' 18"	36	0.2529	735	0.5178	1505	86	1.4740	4197	137.0	± 7.2
98SF-201	SU046-05	37° 49' 36"	121° 50' 54"	10	1.1260	611	3.5710	1937	38	1.4525	4268	87.8	± 4.3
98SF-206	SU046-07	37° 49' 54"	121° 50' 08"	18	0.6082	538	1.3830	1223	63	1.4780	4268	124.2	± 6.7
98SF-209	SU046-08	37° 50' 17"	121° 48' 58"	12	1.3610	692	3.3360	1696	7.4	1.4780	4268	115.7	± 7.1
98SF-210	SU046-09	37° 50' 45"	121° 47' 56"	17	0.9623	971	2.3790	2401	<0.1	1.5034	4268	119.2	± 7.7
98SF-211	SU046-10	37° 50' 37"	121° 48' 12"	26	1.0630	1240	2.8780	3357	6.3	1.5034	4268	106.5	± 4.8
98SF-212	SU046-11	37° 50' 35"	121° 48' 37"	25	1.1890	1047	2.7250	2400	26	1.5288	4268	128.6	± 5.8
98SF-213	SU046-12	37° 51' 09"	121° 47' 14"	27	1.0790	1234	2.7100	3098	1.2	1.5288	4268	115.4	± 5.5
98SF-216	SU046-14	37° 51' 47"	121° 46' 14"	25	0.7907	1409	2.5370	4520	0.2	1.5670	4268	90.7	± 4.2
98SF-219*	SU046-15	37° 54' 32"	121° 45' 51"	14	0.7940	511	2.7610	1777	43	1.5670	4268	86.4	± 4.5
98SF-221	SU046-16	37° 52' 31"	121° 45' 40"	25	1.2200	936	4.2220	3238	0.3	1.5924	4268	89.0	± 5.0
Franciscan Complex Samples													
MD96-1	SU033-16	37° 52' 53"	121° 54' 48"	24	0.7193	479	4.0350	2687	<0.1	1.6770	4639	59.0	± 5.0
MD96-4	SU033-19	37° 52' 32"	121° 55' 43"	29	0.8165	1470	4.3170	7773	<0.1	1.7195	4639	63.0	± 3.0
MD96-7	SU033-22	37° 52' 23"	121° 56' 57"	40	0.6989	1755	3.9000	9794	63	1.7408	4639	59.9	± 1.8
97SF-001	SU040-01	37° 53' 26"	121° 54' 49"	31	0.8726	911	4.0060	4182	0.5	1.3971	4179	60.0	± 3.2
97SF-003	SU040-03	37° 53' 58"	121° 54' 42"	32	0.3712	629	1.6190	2743	15	1.4125	4179	62.2	± 2.9
97SF-004	SU040-04	37° 54' 07"	121° 54' 52"	13	0.5769	106	2.2100	406	54	1.4432	4179	72.3	± 8.0
97SF-005	SU040-05	37° 54' 11"	121° 55' 00"	8	0.2963	53	1.4420	258	58	1.4432	4179	57.2	± 8.9

* Eocene sample.

Note: Abbreviations are: No Xls, number of individual crystals (grains) dated; Rho-S, spontaneous track density (x 10^6 tracks per square centimeter); NS, number of spontaneous tracks counted; Rho-I, induced track density in muscovite external detector (x 10^6 tracks per square centimeter); NI, number of induced tracks counted; $P(\chi^2)$, χ^2 probability (Galbraith, 1981; Green, 1981); Rho-D, induced track density in external detector adjacent to dosimetry glass (x 10^6 tracks per square centimeter); ND, number of tracks counted in determining Rho-D. Age is the sample central fission track age (Galbraith and Laslett, 1993), calculated using zeta calibration method (Hurford and Green, 1983). Analyst: T. A. Dumitru.

The following is a summary of key laboratory procedures. Apatites were etched for 20 s in 5N nitric acid at room temperature. Grains were dated by external detector method with muscovite detectors. Samples were irradiated in well thermalized positions of Oregon State University reactor. CN5 dosimetry glasses with muscovite external detectors were used as neutron flux monitors. External detectors were etched in 48% HF. Tracks counted with Zeiss Axioskop microscope with 100x air objective, 1.25x tube factor, 10x eyepieces, transmitted light with supplementary reflected light as needed; external detector prints were located with Kinetek automated scanning stage (Dumitru, 1993). Only grains with c axes subparallel to slide plane were dated. Ages calculated using zeta calibration factor of 385.9. Confined tracks lengths were measured only in apatite grains with c axes subparallel to slide plane; only horizontal tracks measured (within ±~5-10°), following protocols of Laslett and others (1982). Lengths were measured with computer digitizing tablet and drawing tube, calibrated against stage micrometer (Dumitru, 1993). For the sixteen samples that contained at least 41 measurable confined tracks, angles of confined tracks to the grains' c-axes and the Dpar track entrance diameter where also measured, following protocols of Ketcham and others (1999, 2000), except that confined tracks hosted by surface tracks and by cleavage surfaces were both measured. Age calculations were done with program by D. Coyle.

The following is a summary of thermal history modeling methods. Modeling done with the AFTSolve 1.1.2 program of Ketcham and others (2000). Modeling parameters: (1) used raw track length data (actual lengths, Dpar, and angle to c-axis of each track) and actual track counts (NS, NI, and Dpar of each grain), (2) used annealing model of Ketcham and others (1999) with Dpar kinetic variable; (3) for each sample, divided all data (lengths and track counts) into three kinetic populations based on Dpar such that almost all data fell within the center population, then discarded all but the center population; (4) modeled the center population using its midpoint Dpar value; (5) for length reduction in age standard, used default value of 0.893; (6) for initial track length, used default relations Lom=(0.283)(Dpar)+15.630 µm and Loc=(0.205)(Dpar)+16.100 µm; (7) did not project track lengths to c-axis parallel; (8) calculated 2000 model paths with Monte Carlo scheme, with each path segment monotonic and each segment halved one time, and without enforcing maximum heating or cooling rates; (9) output plots show best single run, good model fit envelope, and acceptable model fit envelope. No adjustments made for slight difference in etching conditions between Ketcham and others (1999, 2000) (20 seconds, 21°C, 5.5 N HNO_3) and our laboratory (20 seconds, room temperature [~22°C], 5.0 N HNO_3), nor for likely minor interlaboratory differences in length reduction in age standard or initial track length relationships.

Unruh et al., Diablo, Table DR2
Microsoft Word 2004 for Mac, v 11.3 file

TABLE DR3. He ANALYTICAL DATA FOR INDIVIDUAL APATITE GRAINS FROM SAMPLES FROM MT. DIA

He ref	Sample and Grain	Grain Desig-nation	U (ppm)	Th (ppm)	He (nmol/g)	Age (Ma) Raw	Grain radius (microns)	Grain length (microns)	Grain mass (µg)	Ft factor	Age (Ma) Ft Corrected
01HRZ	97SF006fn(c)	--	9.320	19.170	0.751	9.984	39.998	351.411	3.019	0.688	14.513
01HSA	97SF006fn(d)	--	1.258	3.674	0.274	23.704	42.855	257.130	2.536	0.692	34.230
01HRX	97SF006fn(a)	--	3.318	9.949	0.820	26.614	57.140	342.840	6.010	0.763	34.848
01HRY	97SF006fn(b)	--	2.993	3.945	1.089	50.896	57.140	325.698	5.710	0.768	66.216
01HRU	97SF006cs(b)	--	2.013	4.494	0.518	30.960	74.282	385.695	11.427	0.814	38.032
01HRV	97SF006md(a)	--	1.725	3.974	0.421	29.091	74.282	291.414	8.634	0.805	36.116
01HRS	97SF006cs(a)	--	1.459	3.317	0.327	26.853	77.139	419.979	13.418	0.821	32.697
01HRW	97SF006md(b)	--	1.793	3.660	0.195	13.518	77.139	325.698	10.406	0.815	16.580
01HQH	98SF201(a)TD	e	37.393	84.819	6.410	20.542	37.141	188.562	1.397	0.645	31.805
01HQI	98SF201(b)TD	f	31.922	61.739	4.999	19.780	39.998	274.272	2.356	0.681	29.030
01HQJ	98SF201(c)TD	g	42.450	50.360	5.431	18.382	45.712	171.420	1.923	0.697	26.350
01HQK	98SF201(d)TD	h	22.549	20.643	5.166	34.594	45.712	308.556	3.462	0.722	47.848
01HQL	98SF201(e)TD	I	27.905	23.193	5.099	28.066	62.854	257.130	5.454	0.779	36.001
01HQM	98SF201(f)TD	j	19.634	43.419	8.126	49.922	68.568	385.695	9.736	0.801	62.271
01HTL	98SF216(a)cs	k	26.353	51.915	6.052	28.819	62.854	299.985	6.363	0.780	36.929
01HTM	98SF216(b)cs	l	5.537	1.286	0.600	18.865	62.854	291.414	6.181	0.786	23.977
01HTN	98SF216(c)fn	m	14.784	38.718	5.092	39.119	45.712	231.417	2.596	0.704	55.469
01HTP	98SF216(d)fn	n	104.291	114.461	6.683	9.368	42.855	171.420	1.690	0.683	13.708
01HRO	98SF212(a)TD	o	25.401	43.007	5.785	29.908	37.141	231.417	1.714	0.657	45.463
01HRP	98SF212(b)TD	p	21.662	23.436	2.027	13.711	37.141	222.846	1.651	0.659	20.800
01HRR	98SF212(d)TD	q	47.752	25.390	7.351	25.127	48.569	359.982	4.559	0.742	33.843
01HRQ	98SF212(c)TD	r	20.078	33.017	3.126	20.631	51.426	248.559	3.529	0.736	28.000
01HTQ	98SF221(a)cs	a	23.336	52.351	3.141	16.199	51.426	222.846	3.164	0.730	22.186
01HTR	98SF221(b)cs	b	21.406	40.834	2.215	13.131	45.712	205.704	2.308	0.703	18.679
01HTS	98SF221(c)fn	c	53.482	125.920	5.339	11.816	37.141	179.991	1.333	0.643	18.368
01HTT	98SF221(d)fn	d	17.031	35.198	2.870	20.836	39.998	188.562	1.620	0.666	31.263
01HQQ	MD96-4 fn(b)	s	14.789	14.072	1.343	13.642	34.284	222.846	1.406	0.638	21.368
01HQP	MD96-4 fn(a)	t	36.149	99.413	5.489	16.948	39.998	145.707	1.252	0.649	26.080
01HQN	MD96-4 cs(a)	u	47.617	127.790	5.251	12.431	45.712	231.417	2.596	0.704	17.646
01HQO	MD96-4 cs(b)	v	5.498	6.949	0.199	5.137	45.712	179.991	2.019	0.699	7.343
01HQW	MD96-7 fn (a)	w	29.825	57.238	4.576	19.427	34.284	171.420	1.082	0.621	31.261
01HQX	MD96-7 fn(b)	x	4.990	18.324	0.902	17.832	39.998	154.278	1.325	0.650	27.421
01HQU	MD96-7 cs (b)	y	4.590	2.616	0.321	11.339	51.426	222.846	3.164	0.738	15.367
01HQT	MD96-7 cs(a)	z	5.198	8.834	0.310	7.848	51.426	222.846	3.164	0.732	10.722
01HRH	DurangoCG1:l	--				30.001					
01HSF	DurangoCG2:l	--				32.169					
01HQG	DurangoLH4:l	--				32.740					

Data collected at California Institution of Technology (U-Th)/He laboratory using standard methods. 4He released by laser heating of individual apatite grains enclosed in unsealed platinum microcapsules. 4He masses determined by quadrupole mass spectrometry, calibrated against 3He spike. U and Th concentrations determined by dissolving grains, adding U and Th isotopic spikes, and analyzing by inductively coupled plasma mass spectrometry. Grain sizes determined by measurement with optical microscope calibrated against stage micrometer. Ft correction factor (Farley et al., 1996) calculated from grain diameter only. Durango apatite standard analyzed as check on analyses.

TABLE DR4. MODELING OF (U-Th)/He AGES FROM THE MT. DIABLO AREA*

Sample Information

Sample Number	98SF-216	98SF-221	98SF-201	98SF-212	MD96-4	MD96-7
Unit	GVG	GVG	GVG	GVG	Franciscan	Franciscan
Stratigraphic Depth (m)	6000 m	5200 m	5300 m	7625 m	---	---

Time-Temperature Points Input into Models for Each Sample

GVG He Start Age**	105 Ma-10°	93 Ma-10°	97 Ma-10°	141 Ma-10°	---	---
GVG Depositional Age	82 Ma-10°	78 Ma-10°	80 Ma-10°	105 Ma-10°	---	---
FC Exhumation Underway	---	---	---	---	65 Ma-100°	<<--same
GVG Start Exhumation	52.5 Ma-40°	52.5 Ma-32°	52.5 Ma-33°	52.5 Ma-56°	---	---
GVG Start Rapid Burial	52 Ma-15°	<<--same	<<--same	<<--same	---	---
Start Slow Burial	40 Ma-30°	<<--same	<<--same	<<--same	<<--same	<<--same
Start Rapid Burial	11 Ma-35°	<<--same	<<--same	<<--same	<<--same	<<--same
Max Burial-Vary Tmax†	3.5 Ma-Vary	<<--same	<<--same	<<--same	<<--same	<<--same
Samples at Surface Today	0 Ma-20°	<<--same	<<--same	<<--same	<<--same	<<--same

Single Grain Data Input into Models and Resulting Fitted Activation Energies (A_e, kcal/mol)

Grain Designations††	k (a-cs)	a (a-cs)	e (a)	o (a)	s (fn-b)	w (fn-a)
Grain Radius (microns)	62.854	51.426	37.141	37.141	34.284	34.284
Measured He Age (Ma)	36.93	22.19	31.81	45.46	21.37	31.26
Fitted A_e for T_{max}=70°C	32.67	32.63	33.27	33.42	33.51	33.97
Fitted A_e for T_{max}=73.73°C	32.96	32.93	33.57	33.67	33.80	34.25
Grain Designations††	l (b-cs)	b (b-cs)	f (b)	p (b)	t (fn-a)	x (fn-b)
Grain Radius (microns)	62.854	45.712	39.998	37.141	39.998	39.998
Corrected He Age (Ma)	23.98	18.68	29.03	20.80	26.08	27.42
Fitted A_e for T_{max}=70°C	32.37	32.69	33.11	32.98	33.52	33.58
Fitted A_e for T_{max}=73.73°C	32.65	32.98	33.40	33.23	33.80	33.86
Grain Designations††	m (c-fn)	c (c-fn)	g (c)	q (d)	u (cs-a)	y (cs-b)
Grain Radius (microns)	45.712	37.141	45.712	48.569	45.712	51.426
Corrected He Age (Ma)	55.47	18.37	26.35	33.84	17.65	15.37

Fitted A_e for T_{max}=70°C	33.50	32.95	32.87	32.88	32.97	32.72	
Fitted A_e for T_{max}=73.73°C	33.81	33.25	33.16	33.13	33.26	33.01	
Grain Designations††	n (d)	d (d-fn)	h (d)	r (c)	v (cs-b)	z (cs-a)	
Grain Radius (microns)	42.855	39.998	45.712	51.426	45.712	51.426	
Corrected He Age (Ma)	13.71	31.26	47.85	28.00	7.34	10.72	
Fitted A_e for T_{max}=70°C	32.58	33.19	33.40	32.70	32.45	32.49	
Fitted A_e for T_{max}=73.73°C	32.88	33.49	33.71	32.95	32.74	32.78	
Grain Designations††			i (e)				
Grain Radius (microns)			62.854				
Corrected He Age (Ma)			36.00				
Fitted A_e for T_{max}=70°C			32.70				
Fitted A_e for T_{max}=73.73°C			33.00				
Grain Designations††			j (f)				
Grain Radius (microns)			68.568				
Corrected He Age (Ma)			62.27				
Fitted A_e for T_{max}=70°C			33.35				**Mean and Range Of All Samples**
Fitted A_e for T_{max}=73.73°C			33.65				
Mean and Range of A_e for Each Sample for Two Different T_{max} at 3.5 Ma							
Mean A_e for T_{max}=70°C	32.78	32.87	33.12	33.00	33.11	33.19	**33.01**
E_a Range for sample	1.13	0.56	0.70	0.72	1.07	1.48	**1.60**
Mean A_e for T_{max}=73.73°C	33.08	33.16	33.42	33.25	33.40	33.48	**33.30**
E_a Range for sample	1.16	0.56	0.71	0.72	1.06	1.47	**1.60**

*Modeling was completed using the program of K. Farley (personal communications, 2003). Remaining parameters used were: Log10Do = 1.50 cm2/s; U = 1.00 ppm; Th = 1.00 ppm (computations are insensitive to actual U and Th); Alpha Ejection ON; Delta-t = 0.50 myrs; N = 8 (2**8 grid points). The activation energies (Ae) were varied by trial and error until the observed He ages were matched.

**The He "Start" Ages for the Great Valley and Eocene samples are the time at which He retention was assumed to begin for each apatite grain. Retention probably began when apatite in the samples first cooled below about 85°C while the apatite grains still resided in rocks in the sediment source areas before they were eroded and deposited into the Great Valley forearc basin. For the modeling, these start ages were assumed to be 5 million years younger than the modeled fission track provenance ages. Those provenance ages approximate the time of cooling of the apatite grains below about 100°C in sediment source areas. Figure FTDR-3B shows the approximate percent resetting exhibited by each apatite grain. Those values were computed as follows: Percent Reset = 100% x (Observed He Age - 3.5 Ma)/(He Start Age - 3.5 Ma). This calculation yields the approximate proportion of the total 4He that had been released from the grain up until and including the time of Tmax at 3.5 Ma.

†Several temperatures at 3.5 Ma were modeled. Results for Tmax = 70°C and 73.73°C are included here.

††Two designations are given, a simplified designation ("a" to "z") used in Figure FT-1 and the designation used during the laboratory measurements (in parentheses).

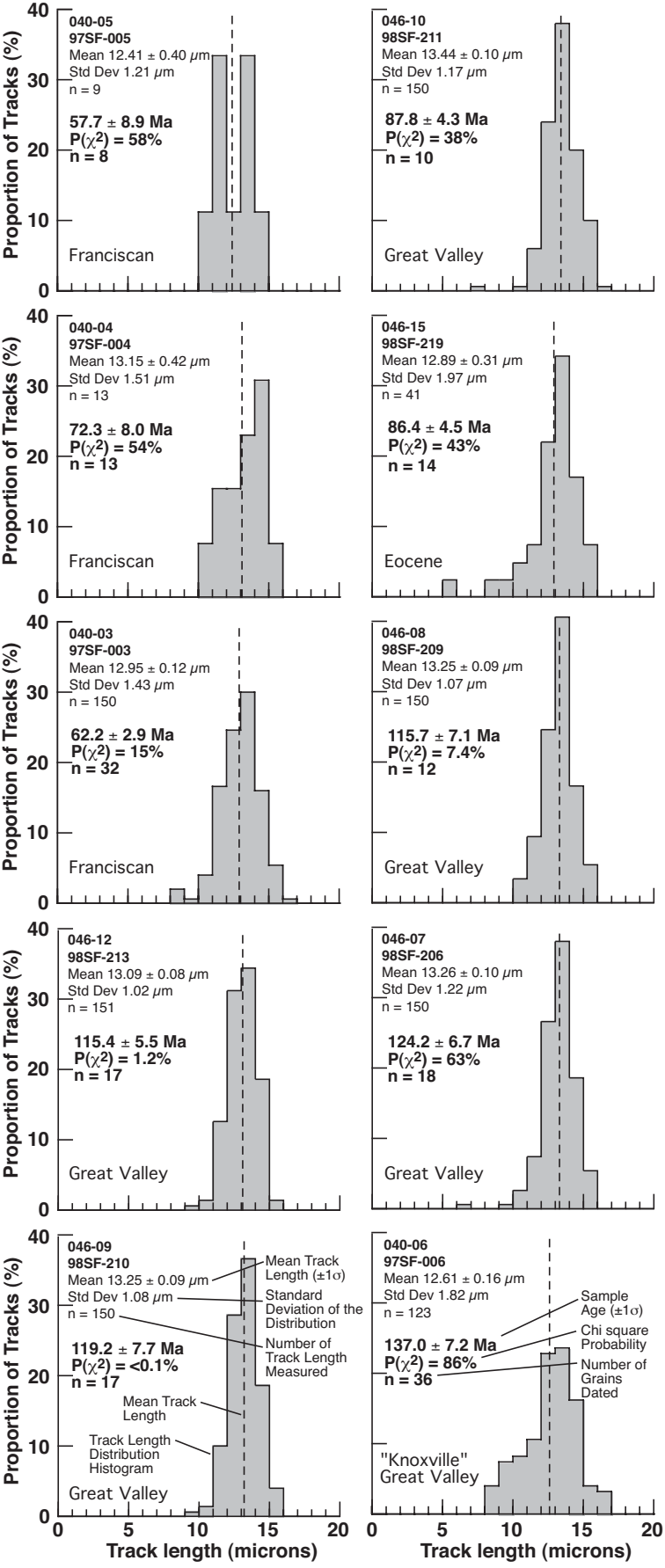

Unruh et al., Figure DR1
Data Repository Only
January10, 2007
Illustrator CS2 file (histograms may have been originally drafted in Canvas v. 3.5?)

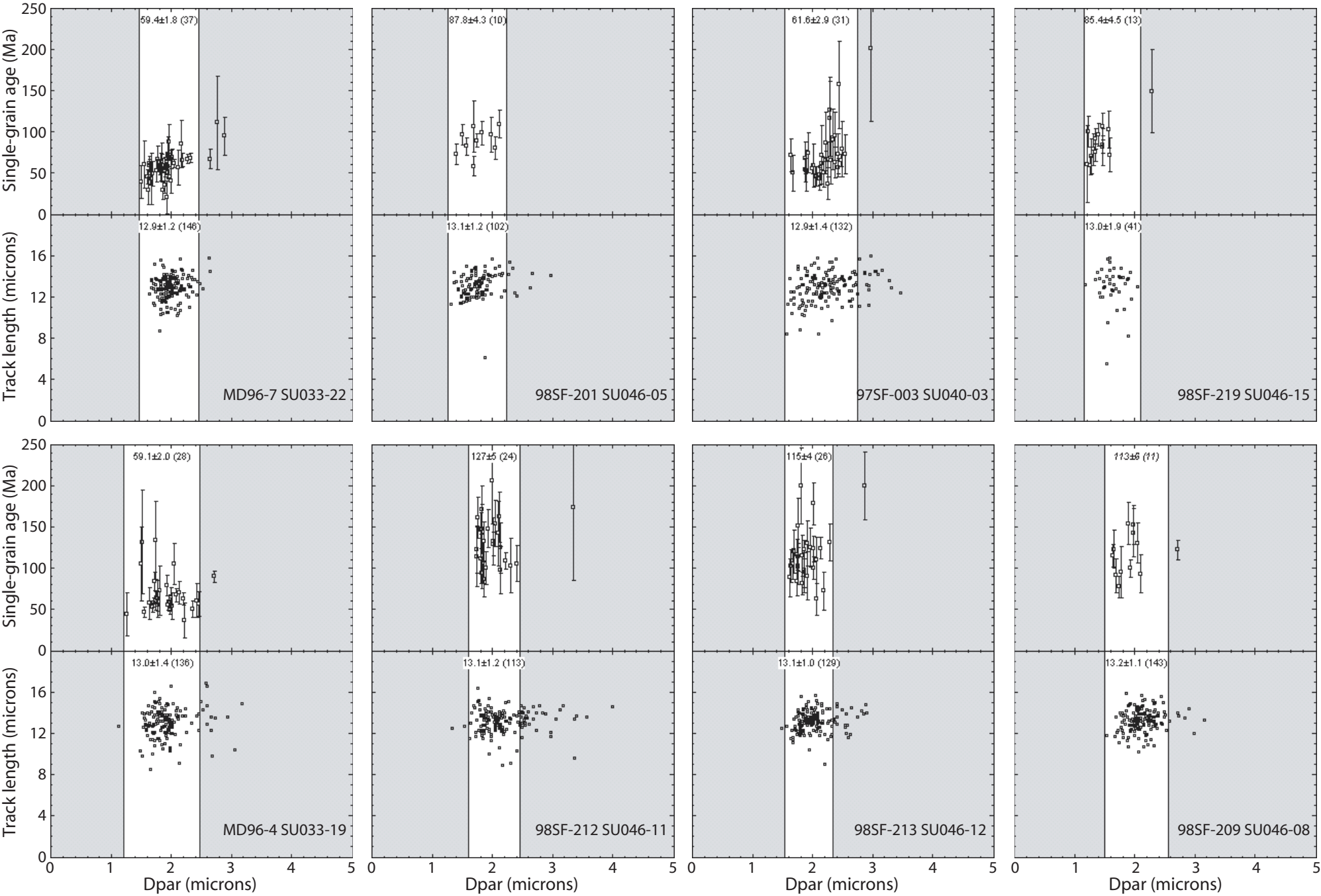

Unruh et al., Diablo, Figure DR2 (page 1 of 2)
10 June 2006; Illustrator CS2 file

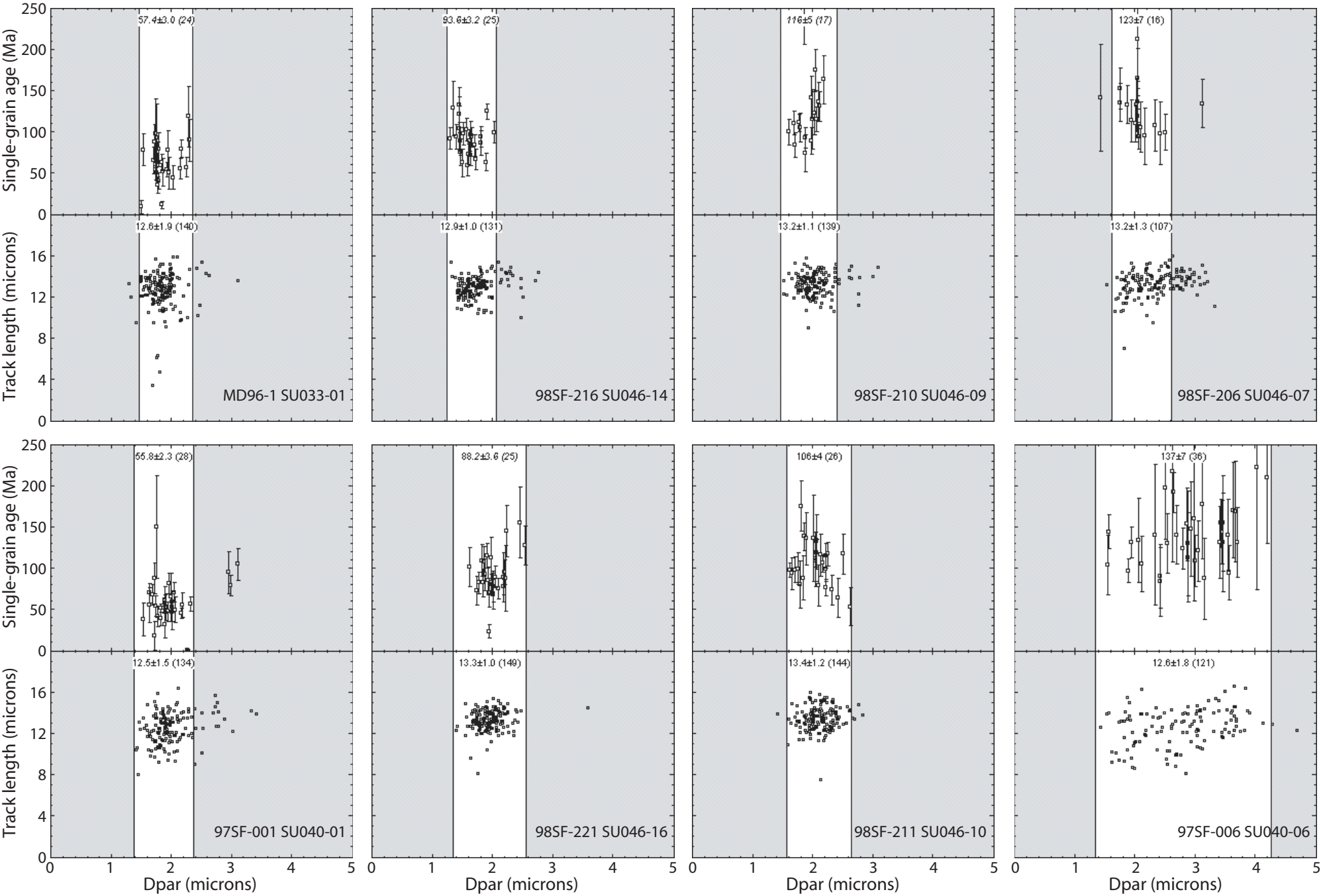

Unruh et al., Diablo, Figure DR2 (page 2 of 2)
10 June 2006
Illustrator CS2 file

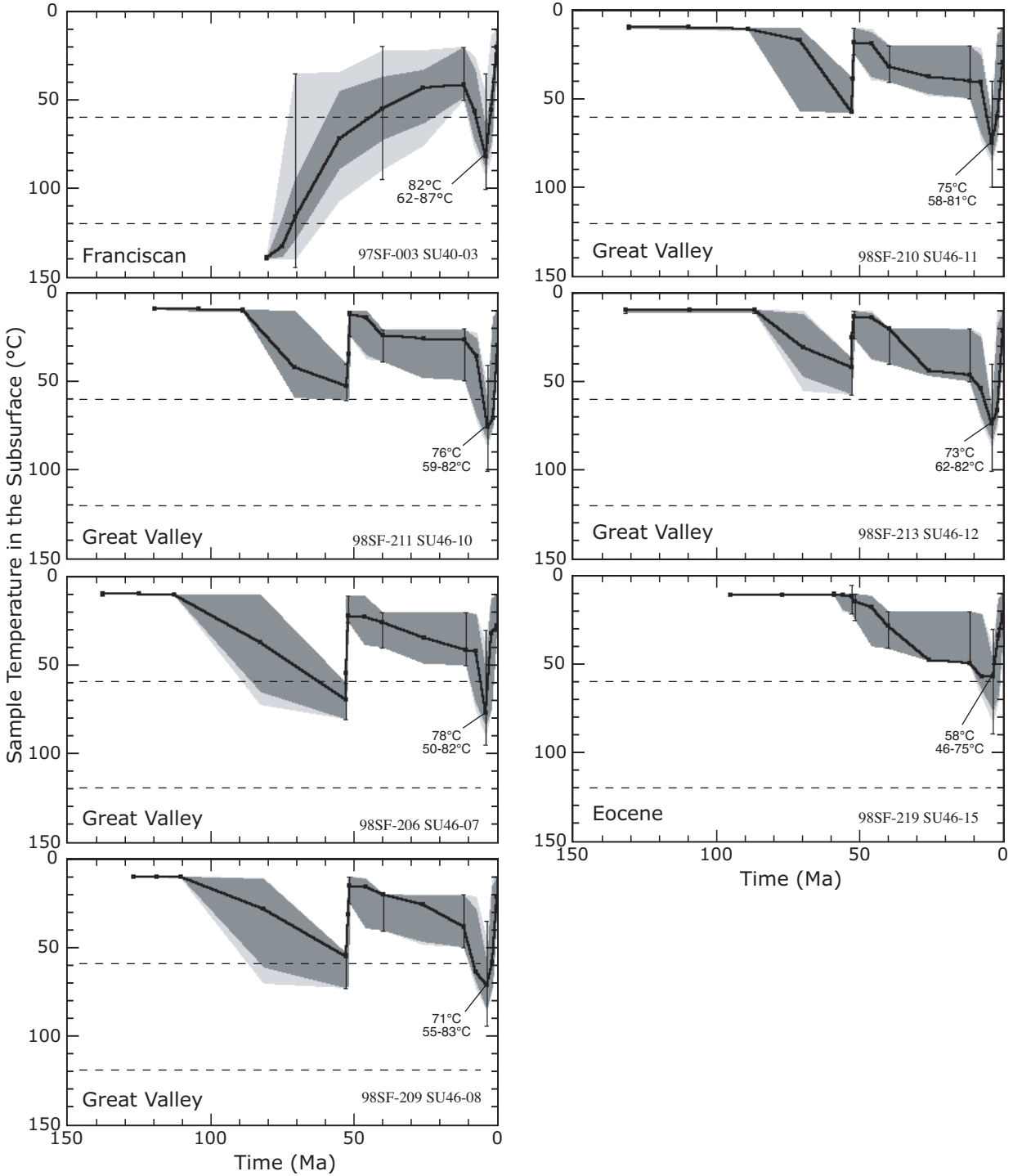

Unruh et al., Figure DR3
Data Repository Only
10 June 2006
Illustrator CS2 file
Contains objects transferred from modeling program screen shots via Photoshop; figure contains two distinct levels of gray shading.

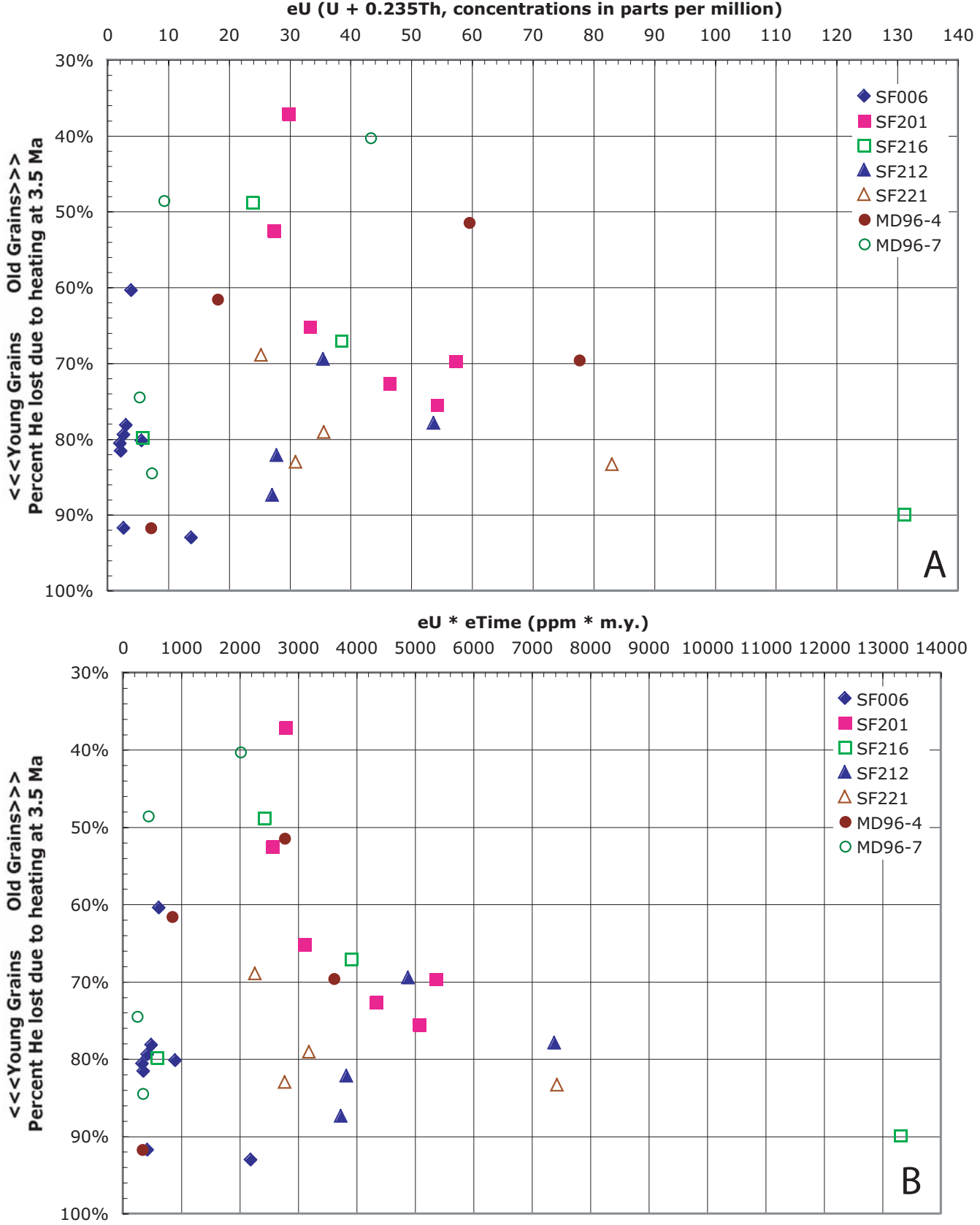

Figure DR4
Unruh et al., Mt Diablo
10 January 2007
Illustrator CS2 file (originally Excel file)
Color symbols may be printed color or black and white

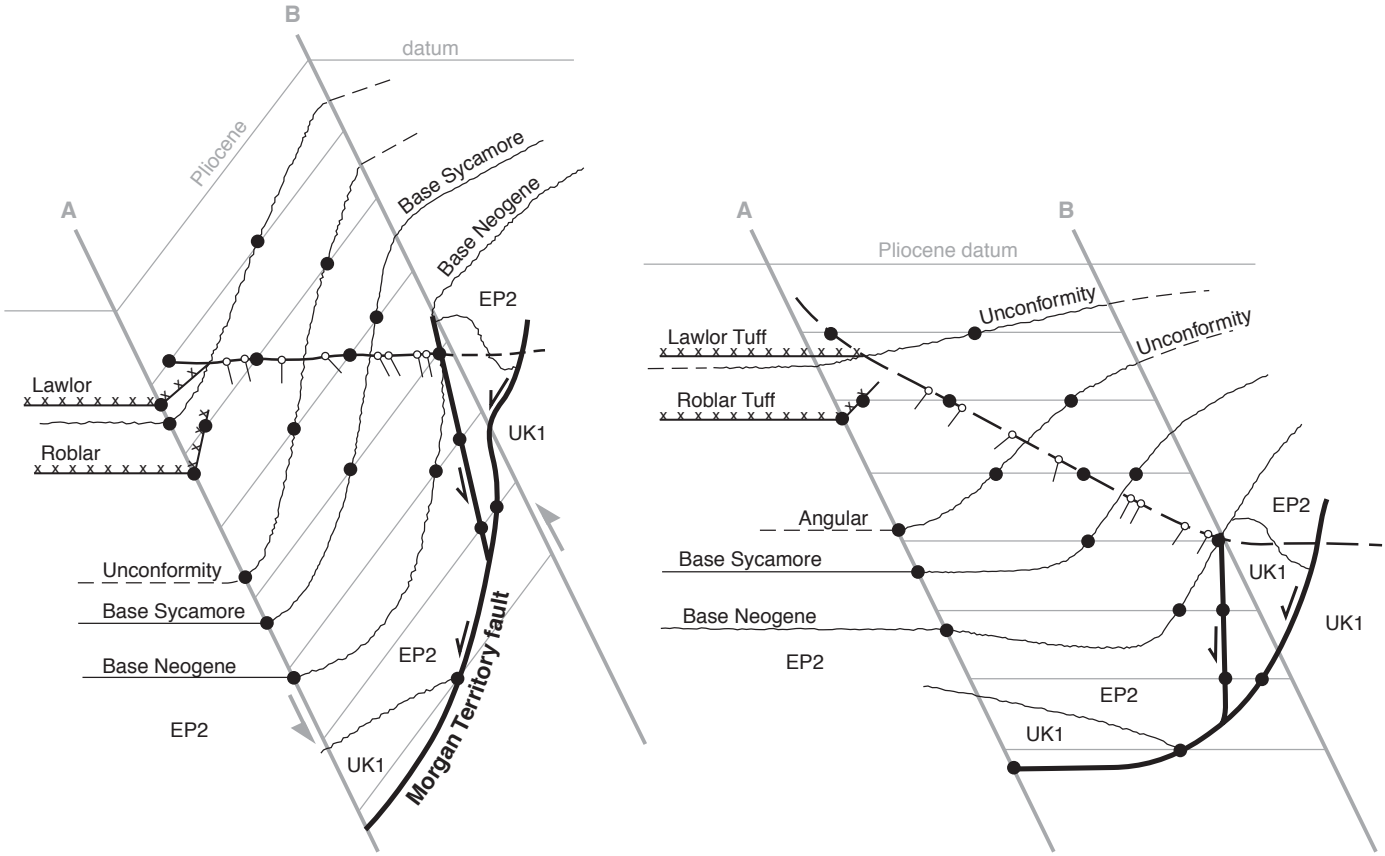

(A) Forelimb of Mt. Diablo anticline

(B) Restored forelimb

Figure DR5: In developing restored cross sections, we assume a kink-band-propagation style of folding (Suppe, 1983; Suppe and Medwedeff, 1990) and account for the effect of distributed simple shear in the fold limbs by using a graphical approach to transform pre-existing faults and bedding contacts from the deformed to the undeformed state. Shearing of fold limbs during deformation is illustrated by comparing the geometry of the parallelogram defined by the A and B hinge lines in the deformed (Panel A) and restored (Panel B) states. We assume that shear during fold growth is accommodated by distributed reverse slip along planes parallel to dip of the fold limb; in general, these planes need not be parallel to bedding. In cross-section, the shear planes are lines of no finite extension. Intersections of bedding, faults and other features with these lines form a grid of points that is used graphically to map the deformed geometry (Panel A) to the restored geometry (Panel B). Although the distances between points along the lines are the same in both the deformed and restored states, the lengths and angular relationships of lines that connect these points between shear planes are different in the two states due to simple shear of the fold limb.

Unruh - Figure DHR
File format: Freehand 11